

Particle transport in a nonuniform flow field: Retardation and clogging

Julio R. Valdes^{a)}

Department of Civil and Environmental Engineering, San Diego State University, San Diego, California 92182

J. Carlos Santamarina^{b)}

School of Civil and Environmental Engineering, Georgia Institute of Technology, Atlanta, Georgia 30332

(Received 29 January 2007; accepted 1 May 2007; published online 12 June 2007)

The authors examine the time delays experienced by migratory particles inside nonuniform flow fields using experimental and numerical methods. Particle trajectories are affected by the particle-fluid density ratio and the flow direction, such that particles may precede or trail the fluid. In flow toward an orifice, the time delay suffered by a single particle is a function of the Froude number Fr and the Archimedes number Ar . When multiple particles are transported radially through a porous medium, time delays manifest through localized annular clogging when $0.05 < Ar^{-1} < 0.15$ and $Fr < 6$. Gradual particle sedimentation occurs when $Ar^{-1} > 1$. Applications include filtration and reservoir fluid extraction. © 2007 American Institute of Physics.

[DOI: 10.1063/1.2748850]

Particles are transported by fluids moving through porous networks in a wide range of processes including filtration,^{1,2} water and oil extractions,^{3,4} and flow in biological systems.⁵ Particle entrapment has important desirable or unwanted consequences in these processes. Thus, proper understanding of the underlying physical mechanisms is necessary for process optimization.

A migratory particle inside a porous medium experiences physical and chemical interactions with the pore surfaces, the fluid, and other particles.⁶ Small particles may be trapped by electrical adhesion to pore surfaces. Larger particles are less affected by electrical forces and are trapped by straining and bridging.^{7,8} Straining occurs when a single particle is larger than the pore throat, whereas bridging takes place when multiple particles interact to form a particulate arch against a pore throat that is larger than a single particle. The likelihood of bridging depends on particle shape and the number of available particles in the vicinity of the pore throat.^{9,10}

The severe reduction in flow conductivity in a porous network due to the excessive retention of migratory particles is referred to as clogging. To satisfy volume conservation, the continuity expression for particle-entrained flow along the axis x is $\partial C_r / \partial t = -v_f \partial C_s / \partial x$, where v_f is the flow velocity, C_r is the concentration of retained particles, C_s is the concentration of suspended particles, and t is time. Clogging typically develops near entry ports when suspensions are pumped in, or near exit ports when fluid extraction prompts particle migration in the porous network. Given that the fluid velocity v_f is highest near ports, it is anticipated that $\partial C_s / \partial x$ is a function of v_f . The following sequence of events is hypothesized for clogging in a porous network. (1) Due to inertial effects, particles deviate from streamlines in tortuous paths and collide with pore walls and neighboring particles. The frequency of collisions increases with the spatial variation in velocity $\partial v_f / \partial x$. (2) The delay between particle and

fluid displacement, herein referred to as “retardation,” increases with increasing v_f . (3) The local concentration of migratory particles in a pore gradually increases, and so does the probability of simultaneous arrivals of multiple particles to pore throats, which leads to particle bridging and clogging. It is therefore suggested that bridging is intimately related to particle retardation in fluid flow.

The transport of large particles by a moving fluid is controlled by three coexisting forces: the buoyant weight, the drag force, and the inertial force. The buoyant weight depends on the mass density of the particle ρ_s and the mass density of the fluid ρ_f , $F_B = \pi d^3 g (\rho_s - \rho_f) / 6$, where g is the gravitational constant and d is the particle diameter. The drag force is proportional to the difference between the fluid velocity and the particle velocity, $F_D = 3 \pi \mu d (v_f - v_p)$, where μ is the fluid viscosity. Finally, the inertial force experienced by a particle migrating along the x direction is the product of its mass m_p and acceleration, $F_I = m_p (\partial v_p / \partial t) = m_p (\partial v_p / \partial x) \times (\partial x / \partial t)$. Therefore, differences in mass density and inherent spatial variations in fluid velocity within the tortuous porous network cause particle deviations from streamlines, collisions, and retardation.

We conducted experiments to study the trajectories of single particles inside a nonuniform flow field. A vertical tube (diameter=300 mm, height=850 mm) with a bottom plate containing a central orifice (diameter $d_o=6.4$ mm) was filled with degassed mineral oil ($\rho_f=863$ kg/m³, $\mu=0.17$ Pa s). For each test, a single spherical particle ($d=3.2$ mm) was released from a location eccentric to the orifice centerline, such that the particle reached terminal velocity far from the orifice (Fig. 1). Particles made of different materials were used to attain various mass density ratios ($\rho_s/\rho_f=1.3, 1.6, 3.2, \text{ and } 6.5$) and tests were repeated for different initial release locations.

The flow through the orifice was kept constant during each test and particle trajectories were recorded with a high speed digital video camera. Experimental particle trajectories, digitized from the captured footage frames (instant resolution <0.5 mm), are shown in Fig. 1 for one release location. Streamlines bend near the orifice. However, the particle

^{a)} Author to whom correspondence should be addressed; FAX: 001-619-594-8078; electronic mail: jvaldes@mail.sdsu.edu

^{b)} Electronic mail: jcs@gatech.edu

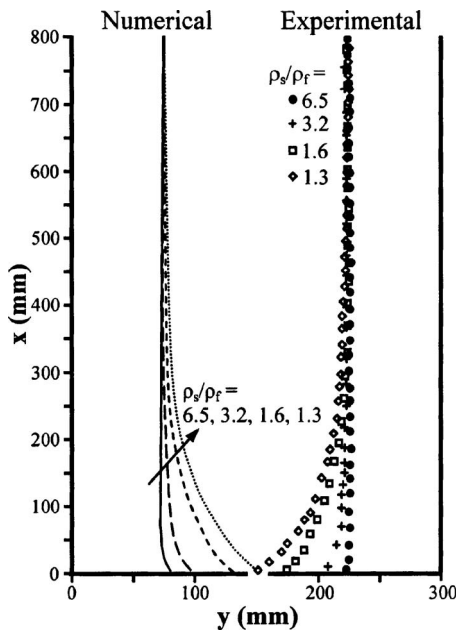


FIG. 1. Numerical and experimental particle trajectories (shown mirrored for clarity).

deviates from the streamlines as inertia and buoyant weight augment the particle’s tendency to follow a vertical downward path.

We extended the experimental study using numerical simulations. The algorithm is a finite-difference solution of Newtonian equations that calculates the trajectory of a particle immersed in a fluid that flows towards an orifice. The following assumptions are made: the particle is spherical, the flow is laminar, and the fluid flow field is not affected by the particle; the particle experiences forces F_D , F_B , and F_I and does not rotate. The numerical formulation proceeds as follows. The fluid velocity field is computed from the solution of Laplace’s equation $\nabla^2 h = 0$, taking into consideration experimental boundary conditions, where h is Bernoulli’s hydraulic head. The instantaneous drag force F_D acting on the particle is calculated as a function of the velocity difference $\mathbf{v}_f - \mathbf{v}_p$. The in-plane particle acceleration components $a_{px} = F_x/m_p$ and $a_{py} = F_y/m_p$ are used to calculate the particle position (x_p^{i+1}, y_p^{i+1}) and velocity $(v_{px}^{i+1}, v_{py}^{i+1})$ at time $t + \Delta t$. The computation stops when the particle collides with a wall or passes through the orifice. The numerical model was validated with results from the experimental test described previously. Figure 1 shows good agreement between the predicted and experimental trajectories for one initial release location. Close agreement was found for all other trajectories.¹¹

We conducted simulations for different flow directions relative to gravity (shown as insets in Fig. 2), far-field fluid velocities (from $v_f = 1$ mm/s to $v_f = 10$ m/s), fluid viscosities ($\mu = 0.001$ Pa s to $\mu = 0.13$ Pa s), and particle sizes ($d = 0.125, 0.167,$ and 0.5 mm, corresponding to orifice-particle size ratios $d_o/d = 2, 3,$ and 4). The time required for the particle to reach the orifice t_p was normalized with respect to the time required for the fluid to reach the orifice t_f . The ratio was assumed to be $\tau = t_p/t_f = \infty$ for particles that collided with walls.

Figure 2 plots the results as a function of the velocity ratio between the particle terminal velocity v_T and the far-field fluid velocity v_f which is the inverse of the Archimedes

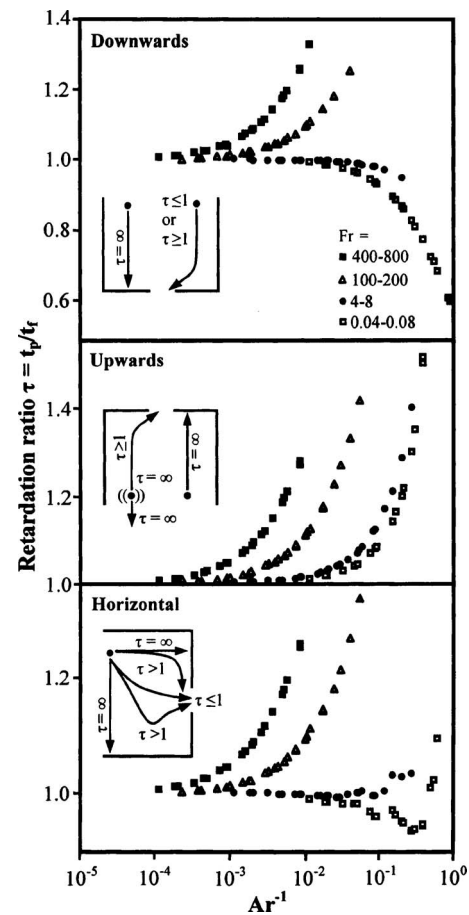


FIG. 2. Results of numerical simulations for single particle transport (each data point denotes a simulation). Insets show observed trajectories for particles with $\rho_s > \rho_f$.

number, $Ar^{-1} = v_T/v_f$. The trends are characterized by specific ranges of the Froude number $Fr = v_f^2/(dg)$, which relates inertial and gravity forces. In downward flow, the viscous drag may be insufficient to align the particle along the streamline and the particle collides with the bottom wall (e.g., when $Ar^{-1} > 0.6$ and $Fr = 5$) or the particle may precede the fluid and pass through the orifice due to the combined gravitational and drag actions (e.g., when $Ar^{-1} < 1$ and $Fr = 0.05$). Lower Ar^{-1} values are required to reduce retardation as Fr increases due to the decreasing ability of the viscous drag to counter the inertial force as streamlines deviate near the orifice. In upward flow, the particle falls downward and never reaches the orifice ($Ar^{-1} > 1$), is dragged upward and passes through the orifice with retardation (e.g., when $Ar^{-1} < 1$ and $Fr = 5$), or collides with the orifice wall (e.g., when $Fr = 100$ and $0.05 < Ar^{-1} < 0.5$). In horizontal flow, a particle initially placed below the central axis of the orifice never precedes the fluid, but a particle located above the centerline may either trail or precede the fluid, as shown in Fig. 2. In the latter case, the particle can either collide with the bottom wall (e.g., when $Ar^{-1} > 0.8$ and $Fr = 5$) or collide with the orifice wall (e.g., when $0.5 < Ar^{-1} < 0.8$ and $Fr = 5$). The particle may precede the fluid when Ar^{-1} and Fr are such that gravity combines with horizontal acceleration to minimize the particle’s travel time; this effect disappears if Ar^{-1} decreases and gravity pulls the particle below the centerline. Although the particle may still reach the orifice, it will do so with significant delay.

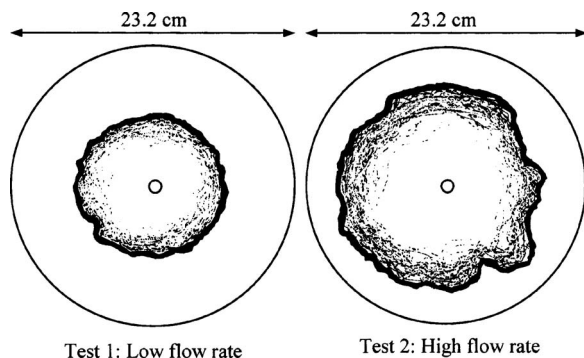


FIG. 3. Final stages of two tests involving multiple particle transport in radial flow (top views). The location of the clogging rings (shown in black) depends on the imposed flow rate, indicating that bridging occurs where sufficient retardation is triggered.

The dependency of retardation on fluid velocity becomes most relevant in radial flow as the mean fluid velocity decreases with radial distance r . We explored potential consequences using a granular monolayer pressed against a transparent acrylic boundary. The model laid flat on a horizontal plane as it was subjected to the radial flow of a particle-entrained fluid. The pore throat to particle size ratio ranged between 0 and 5 to favor bridging. The migratory particles were trapped at a specific radial distance from the extraction point, forming a localized annular clogging pattern. Tests were repeated for different flow rates. Top views of the final stages are shown in Fig. 3. The dark regions denote trapped particle locations. The radial distance from the extraction

point to the clogging ring increased with increasing flow rate, in agreement with velocity-dependent retardation effects analyzed above, which caused particle accumulations that facilitated localized bridging and clogging. Dimensionless ratios Fr and Ar^{-1} are proper scaling parameters: clogging rings occurred when $0.05 < Ar^{-1} < 0.15$ and sedimentation occurred when $Ar^{-1} > 1$.¹² Fr values were below 6 for all tests. Clearly, the migration of multiple particles in a porous network (Fig. 3) is more complex than the migration of a single spherical particle released inside an idealized single-pore setting (Fig. 1). Still, dimensionless parameters Ar^{-1} and Fr provide guidelines to bind possible particle migration regimes in porous networks.

This research was supported by Shell, the Goizueta Foundation, and the U.S. National Science Foundation.

¹J. L. Sherard, L. P. Dunnigan, and J. R. Talbot, *J. Geotech. Engrg.* **110**, 6 (1984).

²S. Datta and S. Redner, *Phys. Rev. E* **58**, 2 (1998).

³T. W. Muecke, *JPT* **31**, 1 (1979).

⁴C. Gruesbeck and R. E. Collins, *SPEJ* **22**, 6 (1982).

⁵S. L. Sanderson, A. Y. Cheer, J. S. Goodrich, J. D. Graziano, and W. T. Callan, *Nature (London)* **412**, 6845 (2001).

⁶L. M. McDowell-Boyer, J. R. Hunt, and N. Sitar, *Water Res.* **22**, 13 (1986).

⁷J. P. Herzig, D. M. Leclerc, and P. Le Goff, *Ind. Eng. Chem.* **62**, 5 (1970).

⁸V. Ramachandran and H. S. Fogler, *J. Fluid Mech.* **385**, 129 (1999).

⁹R. Sakthivadivel and H. A. Einstein, *J. Hydr. Div.* **96**, 2 (1970).

¹⁰G. H. Goldsztein and J. C. Santamarina, *Appl. Phys. Lett.* **85**, 19 (2004).

¹¹J. R. Valdes, Ph.D. thesis, Georgia Institute of Technology, 2002.

¹²J. R. Valdes and C. A. Lestas, *Int. J. Geomech.* **7**, 1 (2007).